A GENERAL COMPUTATIONAL FRAMEWORK FOR DESIGNING MORPHING STRUCTURES

Rainer M.J. Groh[1] and Alberto Pirrera[2]

[1]Bristol Composites Institute (ACCIS), University of Bristol, rainer.groh@bristol.ac.uk
[2]Bristol Composites Institute (ACCIS), University of Bristol, alberto.pirrera@bristol.ac.uk

Keywords: Morphing composites, Nonlinear structures, Bifurcations, Generalised path-following

ABSTRACT

Structural morphing is a bio-inspired design strategy that aims to conform structures to different operating environments, typically by adapting the geometrical shape in a compliant manner. Composites play an enabling role for larger-scale morphing structures as multi-functionality is readily incorporated in the manufacturing process. To date there is no predominantly accepted technique of analysing and designing these structures, especially in a manner that integrates easily with established tools used in industry. One potential candidate in this respect is *generalised path-following*, which combines a numerical continuation algorithm with the geometrical versatility of the finite element method. Morphing composites often take the form of multistable laminates which, as the name suggests, are driven by instabilities. The two (or more) stable states that are exploited in a multistable laminate are typically a product of postbuckling or other forms of prestress, and the ensuing snap-through phenomenon is a catastrophic event (in a mathematical sense) in itself. In this respect, a generalised path-following algorithm is ideally suited for analysing these structures as it is capable of detecting critical instability points, switching to secondary bifurcated branches, and evaluating the parametric response of critical points with respect to any other parameter. We show that the full complexity of multi-snap events of bistable laminates is robustly captured by this algorithm, and that the ability to determine loci of instability points with respect to additional parameters is especially useful for rapid parametric studies.

1 INTRODUCTION

Morphing structures have, for many years, held the promise as the next enabler of weight reductions for the aerospace industry. The premise behind this idea is simple – if structures can be designed to adapt their shape to more optimally conform to different loading conditions, then structural efficiency is improved as a result. In fact, this multi-functionality has a very strong empirical proponent: Nature. Birds, for example, can adapt the camber and angle of attack of their wings to different flight scenarios. Even though some of the concepts found in nature are already being exploited in aircraft structures, such as slats and flaps, they often rely on rigid load-bearing components connected to heavy hydraulic or electric actuators.

Composite materials play a fundamental role in enabling morphing, because their orthotropy can be exploited to design structures with high stiffness in one direction, say the loading direction, and low stiffness in another direction, a potential actuating direction. Hence, composites create the opportunity for servo-elastic tailoring. Furthermore, the laminated nature of advanced composites facilitates a union of materials with dissimilar thermal expansion coefficients, which can be used to build devices that exhibit large-scale shape changes in response to variations in the surrounding temperature [1]. Finally, the geometric nonlinearity of thin-walled shells can be conveniently coupled with the orthotropy of composite materials to design bi- or even tristable shells [2].

To date, the adoption of morphing structures has been hampered by two open research questions:

1. How to design structures and use materials that are sufficiently stiff to reliably carry the operational loads, while simultaneously providing sufficient flexibility for actuation?

2. How to analyse these structures accurately and efficiently, and particularly in a manner that is compatible with accepted methods used in industry?

The second question is especially poignant as confidence in computational tools can serve as an enabler for non-conventional designs. To date, there is no unique way of designing morphing structures. In recent years, particular focus has been on specialised analytical and computational techniques tailored for the analysis of morphing structures [1–7], usually based on the classical *von Kármán* strains (small strains, small displacements and moderate rotations). However, an agreed "best" method has not yet been established. A major drawback of these specialised approaches is that they are often restricted to simple geometries and cannot readily be integrated with the standard tools used in industry, such as the finite element method.

In some cases, commercial finite element packages are used to analyse morphing structures. Most of the time, these analyses are rather *ad hoc*, because structural instabilities that are exploited to design multi-stable structures cannot be treated robustly. Rather, the engineer needs to be aware of possible instabilities and distinct stable configurations *a priori*, and then "coax" the algorithm to land on the required mode shape, using, for example, initial imperfections. Such an approach is ill-suited and computationally prohibitive for preliminary design exploration or parametric studies, and especially not scalable for industrial use. Thus, a more robust modelling framework is needed.

2 GENERALISED PATH-FOLLOWING

The ideal computational framework for morphing structures includes, but is not limited to, the following characteristics:

1. Applicable to arbitrary (thin-walled) geometries.

2. Applicable to large displacements and rotations (e.g. total Lagrangian framework) such that a large variety of structural instabilities are accounted for.

3. Detects critical instability points and allow branch switching onto secondary paths without recourse to initial imperfections.

4. Allows for rapid parametric studies of critical points with respect to any geometric or constitutive parameter.

5. Is readily integrated with accepted computational methods used in industry.

One possible framework that addresses all of these points is the so-called *generalised path-following technique*. In the 1960's Sewell introduced the notion of an equilibrium surface [8], *i.e.* a surface whose shape could be used to identify the stability of the underlying structure with respect to changes in the governing parameters. With the advent of catastrophe theory in structural mechanics this interest intensified, mostly in an analytical setting [9–11], but a generalised computational framework was not introduced until the seminal papers by Rheinboldt [12, 13] in the 1980's. These concepts allowed, for example, loci of bifurcation and/or limit points to be traced directly with respect to any parameter; branch switching between fundamental and bifurcated equilibrium paths; and path-following with respect to any parameter, *e.g.* thickness, Young's modulus, dimensions, *etc*. Starting from the mid 1990's, Eriksson and co-workers [14, 15] established themselves as the main proponents and developers of generalised path-following, presenting numerous examples where the approach proved to be of great benefit, while also providing details on how the technique could be incorporated into commercial nonlinear finite element codes. More recently, the technique has been successfully applied to the analysis of bi-stable plates and shells for morphing structures [6].

3 THEORY

A generalised path-following algorithm couples a numerical continuation solver that is capable of detecting critical instability points, switching to secondary bifurcated branches and evaluating the parametric response of critical points with respect to any other variable, with the versatility of the finite element method. Hence, the term *generalised path-following* refers to the fact that any arbitrary curve, *e.g.* fundamental path, bifurcated path, locus of critical points, *etc.*, on a nonlinear equilibrium surface, can be traced using an arc-length solver.

The conventional equilibrium of internal and external forces can be expressed as a function of a loading parameter, λ, and the displacement state variables, $\boldsymbol{u}$, in the form:

$$\boldsymbol{F}(\boldsymbol{u}, \lambda) = \boldsymbol{f}(\boldsymbol{u}) - \boldsymbol{p}(\lambda), \tag{1}$$

where $\boldsymbol{p}(\lambda)$ is the external (non-follower) load vector and $\boldsymbol{f}(\boldsymbol{u})$ is the internal force vector. For generalised path-following, Eq. (1) is adapted to incorporate any number of additional parameters, such that,

$$\boldsymbol{F}(\boldsymbol{u}, \boldsymbol{\Lambda}) = \boldsymbol{f}(\boldsymbol{u}, \boldsymbol{\Lambda}_1) - \boldsymbol{p}(\boldsymbol{\Lambda}_2), \tag{2}$$

where $\boldsymbol{\Lambda} = [\boldsymbol{\Lambda}_1^\top, \boldsymbol{\Lambda}_2^\top]^\top = [\lambda_1, \ldots, \lambda_p]^\top$ is a vector containing p control variables. $\boldsymbol{\Lambda}_1$ corresponds to parameters that influence the internal forces (*e.g.* material properties, geometric dimensions, temperature and moisture fields) and $\boldsymbol{\Lambda}_2$ relates to externally applied mechanical loads (*e.g.* forces, moments, tractions).

The n number of equilibrium equations in Eq. (2), correspond directly to the n number of displacement degrees of freedom in the system. Because the structural response is parametrised by p additional parameters, a p-dimensional solution manifold in $\mathbb{R}^{(n+p)}$ exists – the so-called *equilibrium surface*. By defining additional auxiliary equations, $\boldsymbol{g}$, specific solution subsets on the p-dimensional solution manifold are defined. Hence, we wish to evaluate solutions to the augmented system

$$\boldsymbol{G}(\boldsymbol{u}, \boldsymbol{\Lambda}) \equiv \begin{pmatrix} \boldsymbol{F}(\boldsymbol{u}, \boldsymbol{\Lambda}) \\ \boldsymbol{g}(\boldsymbol{u}, \boldsymbol{\Lambda}) \end{pmatrix} = \boldsymbol{0}. \tag{3}$$

For r auxiliary equations, the solution to Eq. (3) becomes $(p - r)$-dimensional and hence $p - 1$ auxiliary equations are required to define a one-dimensional curve, or so-called *subset curve* of the multi-dimensional solution manifold. As outlined by Eriksson [15] these subset equations can define fundamental equilibrium paths (the fundamental load parameter is varied from the original unloaded state); parametric equilibrium paths (a non-load parameter is varied); bifurcation branches emanating from any other equilibrium path; critical paths where the tangential stiffness matrix is singular; paths that define a specific optimality criterion; *etc*.

Only one-dimensional curves are evaluated herein, and therefore $r = p-1$. This means one additional constraining equation is needed to uniquely solve the system of equations for a solution point $\boldsymbol{v} = (\boldsymbol{u}, \boldsymbol{\Lambda})$ on the curve described by $\boldsymbol{G}(\boldsymbol{v})$. Hence,

$$\boldsymbol{G}^N(\boldsymbol{v}) \equiv \begin{pmatrix} \boldsymbol{F}(\boldsymbol{v}) \\ \boldsymbol{g}(\boldsymbol{v}) \\ N(\boldsymbol{v}) \end{pmatrix} = \boldsymbol{0}, \tag{4}$$

where N is a scalar equation which plays the role of a multi-dimensional arc-length constraint along a specific subset curve. A specific solution to Eq. (4) is determined by a consistent linearisation coupled with a Newton-Raphson algorithm, *i.e.*

$$\boldsymbol{v}_{j+1} = \boldsymbol{v}_j - \left(\boldsymbol{G}^N_{,\boldsymbol{v}}(\boldsymbol{v}_j)\right)^{-1} \cdot \boldsymbol{G}^N(\boldsymbol{v}_j) \tag{5}$$

with

$$\boldsymbol{G}^N_{,\boldsymbol{v}} = \begin{bmatrix} \boldsymbol{F}_{,\boldsymbol{u}} & \boldsymbol{F}_{,\boldsymbol{\Lambda}} \\ \boldsymbol{g}_{,\boldsymbol{u}} & \boldsymbol{g}_{,\boldsymbol{\Lambda}} \\ N^\top_{,\boldsymbol{u}} & N^\top_{,\boldsymbol{\Lambda}} \end{bmatrix} \tag{6}$$

where j corresponds to the j^{th} increment and the comma notation has been used to denote differentiation.

As an example, consider the snap-through equilibrium path of a centrally loaded toggle frame with clamped ends as shown in Fig. 1a (or see Eriksson [14]). The toggle frame initially deforms symmetrically on the fundamental equilibrium path but this deformation mode becomes unstable at a symmetry-breaking bifurcation just before the maximum point on the curve – a so-called limit point. In the absence of the bifurcation point, the fundamental equilibrium path becomes unstable at this limit point and the structure snaps dynamically into an inverted stable shape while maintaining symmetry. In the case presented here the toggle frame reaches a subcritical pitchfork bifurcation prior to this limit point, and because the connected asymmetric bifurcation branch is unstable, the toggle frame snaps dynamically into the inverted stable shape by means of this asymmetric mode. As shown in Fig. 1a, the generalised path-following algorithm detects and then computes the location of all critical points exactly (to within a predefined numerical precision) and then automatically branches onto the bifurcated path to provide a complete picture of the nonlinear behaviour. Note that no units are provided for this particular example, because they are arbitrary for the purposes of illustrating the general concepts behind generalised path-following.

Fig. 1a restricts path-following to the classical displacement-load space. To illustrate generalised path-following capabilities, Fig. 1b extends the analysis to changes in the height, H, of the toggle frame. Fig. 1b shows an isometric view in displacement-load-height space of the fundamental and bifurcation paths discussed above, and two additional parametric paths. For these parametric paths, the applied load is held constant at $P = 37.4$ and $P = 64.8$ and the relationship between height (H) and central displacement (w) traced using an analogous arc-length solver. These parametric paths can be useful when, for example, the design load on the toggle frame is known and fixed, and changes in the displacement want to be explored as a function of the toggle frame height, or in fact, any other arbitrary parameter.

Similarly, by imposing a criticality condition in the generalised path-following algorithm, the locus of limit and bifurcation points can be traced, illustrating how changes in the height of the toggle frame effect the load-displacement coordinates of these critical points. The utility of critical paths is threefold. First, they can be used to identify interesting points, such as the coincidence of limit and bifurcation points — so-called hilltop-branching points — or points at which the bifurcation and limit points cease to exist ($H = 0.506$ and $H = 0.346$, respectively) – so-called cusp catastrophes. These points are clearly marked in the orthographic projections of Fig. 1c (w vs. H) and Fig. 1d (P vs. H). Second, critical paths can be used in design studies to determine the sensitivity of bifurcation and limit points with respect to design parameters without having to perform computationally expensive parametric studies. Finally, critical paths can be used for optimisation purposes. For example, as shown in Fig. 1c, the displacement at the first instability load can be maximised by reducing the height of the toggle frame to coincide with the hilltop-branching point ($H = 0.567$).

4 BISTABLE PLATES FOR MORPHING APPLICATIONS

The main aim herein is to show that generalised path-following is particularly well-suited to modelling and designing morphing structures of arbitrary geometry, loading and constitutive properties. Because critical points of instability are not isolated explicitly in commercial finite element codes, current methods require *a priori* knowledge of symmetry-breaking bifurcations such that the connected bifurcation branch can be traced by means of initial imperfections determined from the eigenmodes of a linear eigenvalue analysis. Such an approach is found wanting when (a) the fundamental path is nonlinear, or (b) the structure undergoes secondary bifurcations on the bifurcated path.

As shown in the previous section, branch switching is handled automatically and when required by the generalised path-following algorithm, and this capability is illustrated here by means of a classical example problem from the literature (see Hyer [16] and Pirrera *et al.* [6]). A flat asymmetric cross-ply laminate that is cooled-down from cure to room temperature initially deforms into a saddle-like shape but very soon bifurcates into one of two cylindrical solutions. At room temperature, the ensuing cylindrical

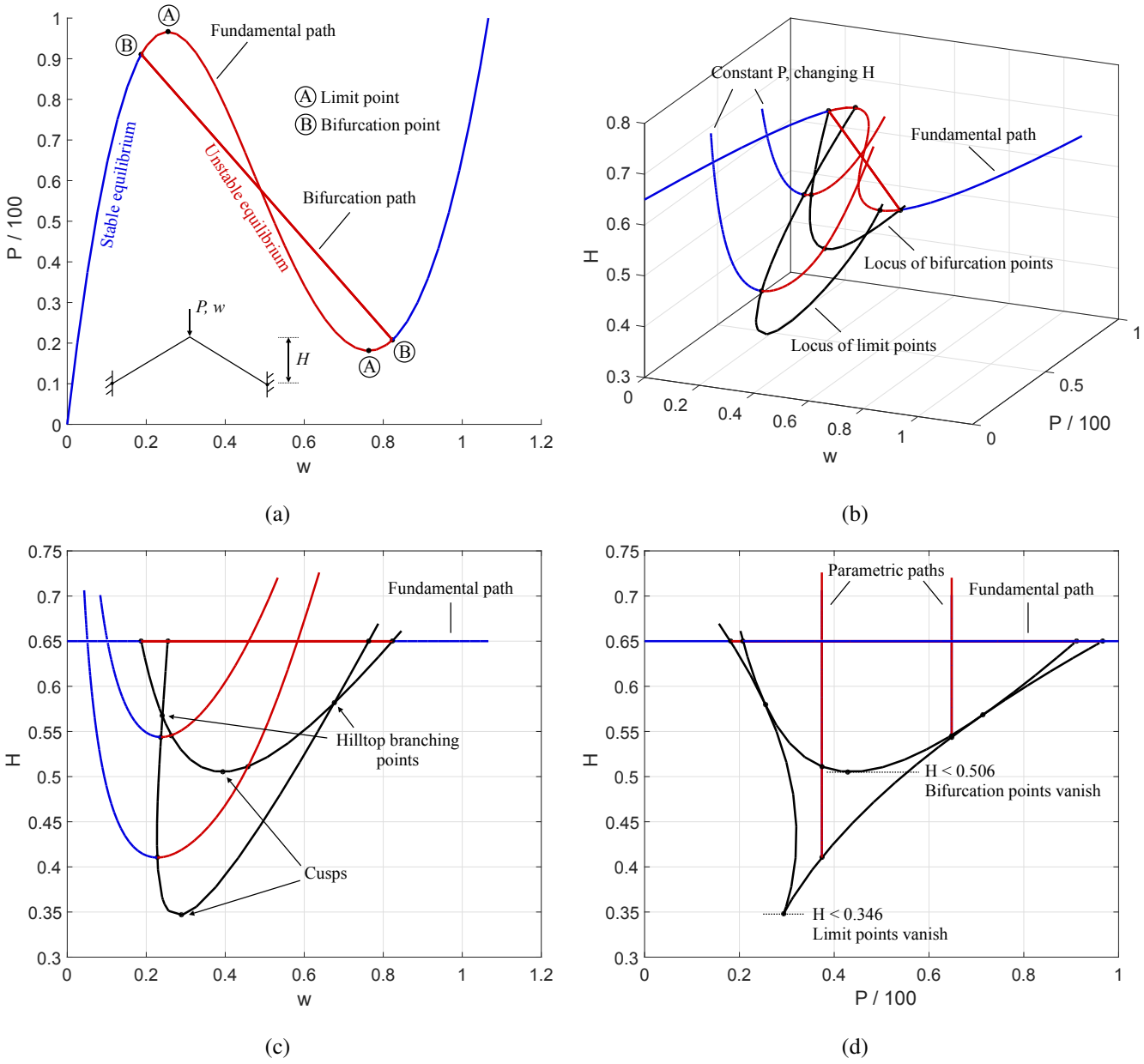

Figure 1: (a) Fundamental and bifurcation equilibrium paths of load (P) versus central displacement (w) for a toggle frame of height $H = 0.65$; (b) Isometric view of the fundamental and bifurcation paths in displacement-load-height space with two additional parametric paths that show the relationship between height (H) and central displacement (w) at applied loads of $P = 37.4$ and $P = 64.8$, and the locus of limit and bifurcation points with changing height. All paths were traced by a single call to the generalised path-following algorithm without recourse to extensive parametric studies; (c) and (d) Orthographic projections of (b) in displacement-height and load-height space, respectively, that clearly denote cusp catastrophes and hilltop-branching points. (Note, no units are shown on the axes here, because for illustrative purposes, the magnitudes of displacement, force and height are arbitrary. Rather, what we wish to demonstrate are the capabilities of generalised path-following.)

Table 1: Typical material properties for a carbon/epoxy composite

E_{11} [GPa]	E_{22} [GPa]	υ_{12} [-]	G_{12} [GPa]	α_{11} $\left[K^{-1}\right]$	α_{22} $\left[K^{-1}\right]$	Ply thickness [m]
161	11.38	0.32	5.17	-1.810 $\times 10^{-8}$	31.0 $\times 10^{-6}$	0.1311 $\times 10^{-3}$

panel can be snapped from one cylindrical shape into its inverted counterpart, thereby creating a bistable plate that is useful for morphing applications. The associated snap-through behaviour is intricate with multiple instability points, and its full complexity is exposed here for the first time.

Consider a four-layer $[90_2/0_2]$ square carbon/epoxy plate with material properties shown in Table 1, generic in-plane dimensions $L_x = L_y$ and fully clamped at its planar midpoint. As a baseline model we assume that panel dimensions $L_x = L_y = 0.25\,\mathrm{m}$, although the effect of varying these dimensions is investigated later. The composite laminate is discretised into a 43×43 node mesh of 196 fully integrated 16-node, total Lagrangian shell elements using the shell director parametrisation of Ramm [17] (two rotations per node, no drilling around director). The effects of shear and membrane locking is minimised by using cubic isoparametric interpolation functions and by refining the mesh sufficiently until convergence with respect to the results by Pirrera *et al.* [6] is obtained, who used a 51×51 node mesh of 2500 reduced integration 4-node `S4R` elements in the commercial finite element software ABAQUS.

As a first load step, the post-cure cool-down of the originally flat $[90_2/0_2]$ laminate from 200°C to room temperature of 20°C is simulated. Figure 2a shows the behaviour of the laminate in terms of the absolute value of the change in temperature $|dT| \in [0, 180]\,\mathrm{K}$ and the out-of-plane displacement w of one of the corners of the laminate. On the fundamental equilibrium path the laminate cools into a saddle shape with zero transverse deflection of the corners. However, this fundamental saddle shape soon becomes structurally unstable at a temperature change of $dT = -4.15\,\mathrm{K}$. The mode shape associated with this bifurcation point is a half-cylinder meaning that, as cooling proceeds, the laminate transitions smoothly and in a structurally stable manner from the initial saddle shape into a semi-cylinder at room temperature. By nature of being a symmetric pitchfork bifurcation, this cylindrical shape can take one of two shapes, up or down, and in reality the final shape depends on initial imperfections. As shown in Figure 2a there are further bifurcation points on the fundamental saddle-shape path but because the branches emanating from these points are all structurally unstable, they are not explored in more detail herein. However, as is shown later, these additional bifurcation points are important for the snap-through behaviour.

Upon cooling to room temperature ($dT = -180\,\mathrm{K}$), snap-through from one cylindrical shape (up or down) to the other (down or up, respectively) is initiated by applying a transverse point load at each of the four corners of the laminate. In the generalised path-following algorithm this loading is readily incorporated as an additional parameter such that the load-displacement plot of snap-through can be superimposed on the previously defined pitchfork diagram. Figure 2b shows this plot in three dimensions, with the transverse force F at one corner plotted versus the associated transverse displacement w at room temperature $dT = -180\,\mathrm{K}$. The load-displacement diagram shows the typical characteristics of a bistable structure with three displacement-axis intercepts, two stable and one unstable, and the necessary limiting hilltops where the structure loses stability and snaps from one stable shape to the other. Inset A of Figure 2b confirms the computational findings of Pirrera *et al.* [6] and the experimental findings by Potter *et al.* [18] that snap-through is here characterised by a multi-snap event – the equilibrium path reaches a first limit point (L1) causing it to snap to the adjacent stable region, at which point the load increases slightly before the structure loses stability entirely and snaps into the inverted shape. Contrary to the computational findings by Pirrera *et al.* [6] this loss of stability does not occur at the second maximum (L3) but at a preceding bifurcation point (B1). The semi-analytical Ritz model by Pirrera *et al.* used the continuation solver EPCONT but bifurcation point (B1) was not evaluated by the solver due to symmetry conditions imposed on computational efficiency grounds. On the contrary, the ABAQUS model used by

the same authors simply did not posses the capabilities to detect this bifurcation point. In fact, inset A of Figure 2b shows two further bifurcation points (B2) and (B3) that are here determined for the first time. Finally, inset B shows a fourth limit point (L4) in the region of the unstable self-equilibrated state of zero applied corner force and zero corner displacement. Due to the symmetry between the two cylindrical deformation modes it is no surprise that the snap-through equilibrium path is symmetric about the origin. Therefore, the four limit points and three bifurcation points have corresponding inverted points which in the following are identified by the letter "i", *e.g.* (L1i), (L2i), (B1i), etc., and referred to as "inverted analogues".

The branches emanating from bifurcation points (B1), (B2), (B3) and their inverted analogues are now explored in detail. Figure 2c shows the bifurcation branch emanating from (B1) which connects to the corresponding bifurcation point (B1i) of the inverted cylindrical shape. This bifurcation path is unstable throughout, apart from a very localised region close to, but disconnected from, (B1) and (B1i). Furthermore, the regions of the curve close to (B1) and (B1i) are tangled and punctured by multiple other limit and bifurcation points. It would be possible to explore the secondary branches emanating from these bifurcation points, but as most of these are likely to be unstable and only add further complexity to the equilibrium diagrams, they are not continued further in this work. Figure 2d presents the path branching from bifurcation point (B2). This branch does not connect to its inverted analogue (B2i) but to (B3i) instead. An identical path mirrored about the origin (symmetric about both axes) also exists which connects (B2i) with (B3), thereby maintaining the expected symmetry of the bifurcation points. These bifurcation branches are again quite tangled close to points (B2) and (B2i), and multiple secondary bifurcation points exist that are not explored further herein. However, there exist six localised regions that are structurally stable. The mode shapes for the two centrally located regions on either side of $w = 0$ are shown and these are rotationally out-of-phase by 180 deg. The six localised regions of stability are surrounded by unstable regions and can, in an experimental setting, not be reached by simply increasing the applied loading. Instead, a force of 1 N could be applied to all four edges and the laminate then forced manually into the depicted mode shape by hand or ideally using a mould. Forcing the structure into this shape requires traversal of an energy hump, but once the required energy threshold has been passed, the laminate should naturally snap into the envisioned structures.

Given the unstable nature of the depicted bifurcation paths the reader might be led to believe that information regarding these paths is of no use to the practising engineer. However, it is well known that such subcritical bifurcations can lead to localisation phenomena [19] and/or extreme sensitivity to initial imperfections [9] that can detrimentally effect the load carrying capability of the structure. Hence, an awareness of the existence of unstable bifurcation branches is necessary if such bistable laminates are to be used safely and reliably in engineering design.

A pertinent question to ask at this point is how the multistability of the laminate changes with temperature. Hence, if the laminate only cools to $50°$C rather than to room temperature, then how is the snap-through behaviour affected? As the snap-through behaviour is governed by limit and bifurcation points on the snap-through equilibrium path, we can use the limit point and bifurcation point continuation capability to determine how each of the previously identified points (L1)-(L4), (B1)-(B3) and their inverted analogues change with temperature. Indeed, Figure 3a reveals that many of these points are directly related to bifurcation points on the fundamental cool-down path of Figure 2a. Individual limit point and bifurcation point loci are shown in more detail in Figures 3b-3d.

Figure 3b shows that limit point (L1) and its inverse analogue (L1i) arise as a direct continuation of the first bifurcation point on the fundamental cool-down path. This is not surprising as without cooling beyond this first critical temperature, the two cylindrical shapes do not exist, and hence there is no snap-through. It is also evident that the transverse corner forces at limit loads (L1) and (L1i) increase monotonically in magnitude with increased post-cure cooling, meaning that the greater the degree of post-cure cooling, the greater the required force to snap between the two cylindrical shapes. Furthermore, limit points (L1) and (L1i) remain the first critical instability points throughout the entire temperature range and are therefore expected to initiate snap-through at all times.

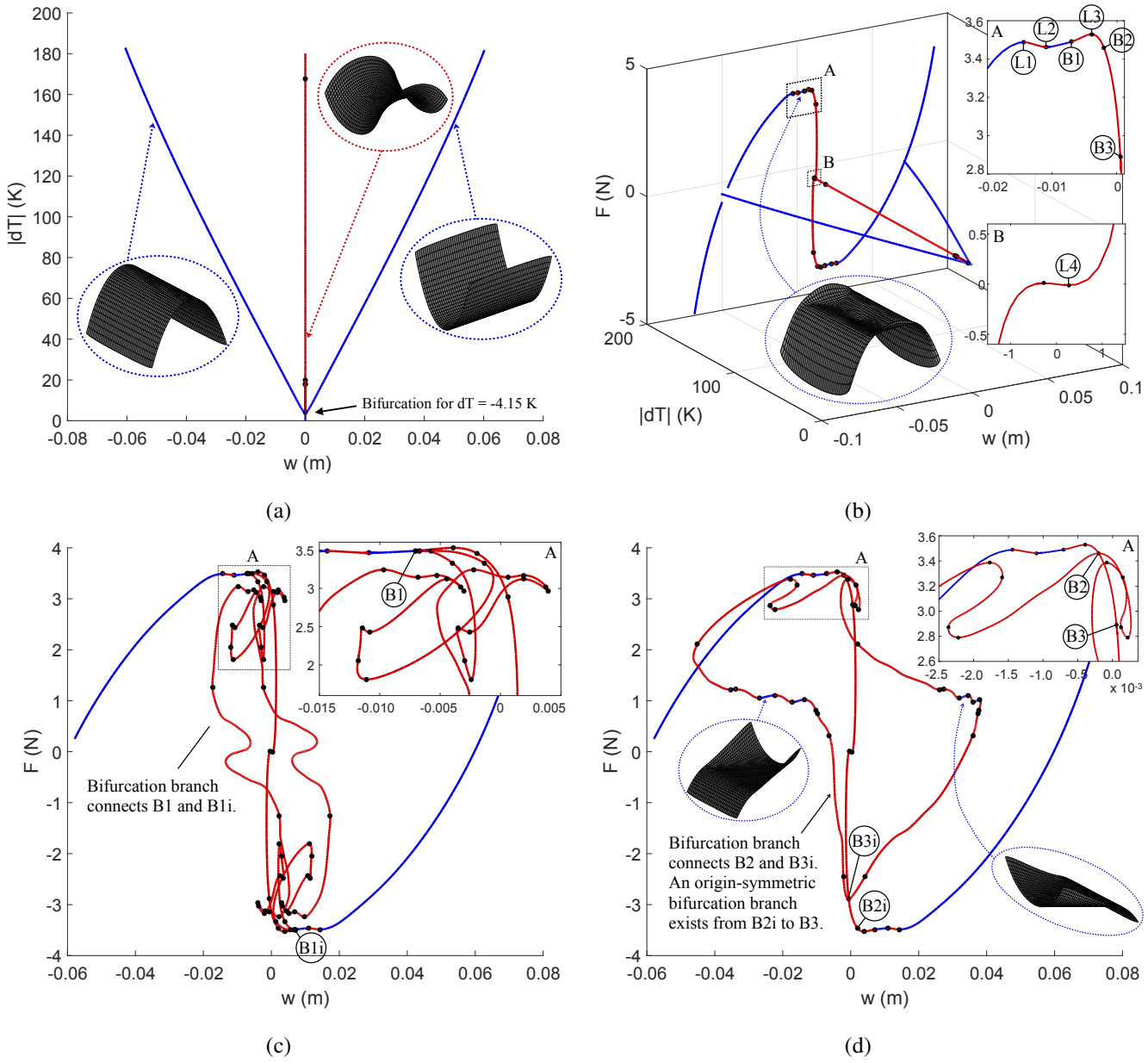

Figure 2: (a) Pitchfork bifurcation diagram of an unsymmetric $[90_2/0_2]$ laminate. Upon cool-down from cure temperature at 200°C the laminate initially deforms into a saddle shape, but this deformation mode is structurally unstable beyond a change in temperature of -4.15 K. Beyond this temperature a symmetry-breaking cylindrical shape is added as a perturbing eigenmode such that at room temperature of 20°C the laminate takes one of two cylindrical mode shapes. (b) Snap-through diagram from one cylindrical shape to the inverted cylindrical shape at room temperature. As the inset shows the snap-through event is not governed by a simple limit point. Rather the panel loses stability at (L1) and then finally snaps to the inverted shape at bifurcation point (B1). (c) Snap-through equilibrium path with additional bifurcation branch connecting bifurcation point (B1) and its symmetrically inverted analogue (B1i). (d) Snap-through equilibrium path with additional bifurcation branch from (B2) to (B3i). The bifurcation branch includes six localised stable regions with two of the associated deformation modes shown.

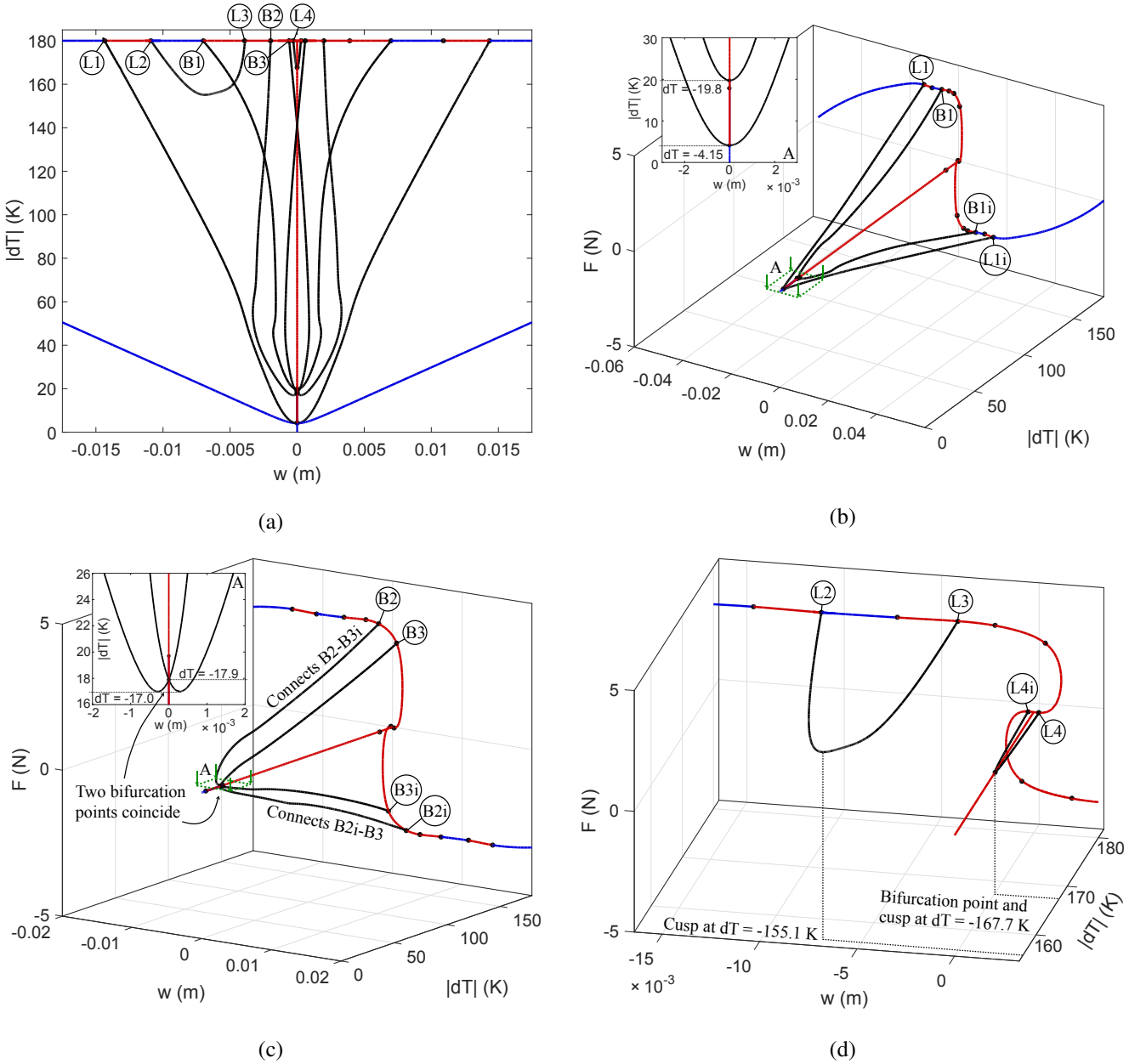

Figure 3: (a) Locus of all limit points (L1)-(L3), bifurcation points (B1)-(B3) and their inverted analogues with varying cool-down temperature. (b)-(d) Detailed plots of limit point and bifurcation point loci with individual features of interest.

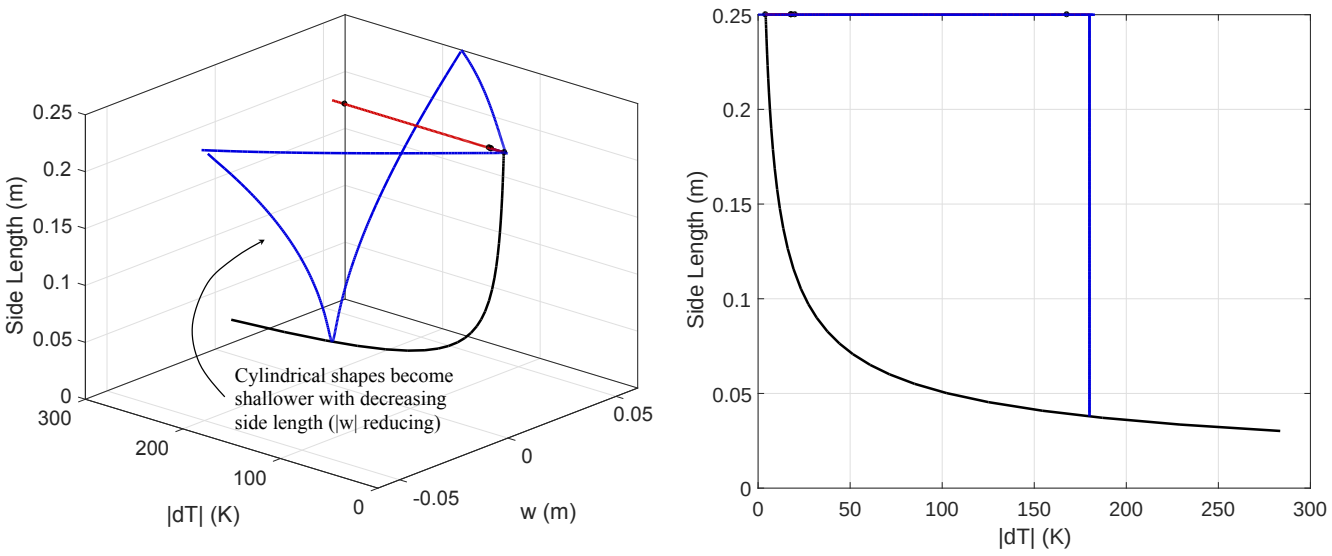

(a) (b)

Figure 4: (a) Isometric view of the locus of first instability points on the fundamental cool-down path with changing laminate side length. The plot also shows that the two cylindrical shapes become shallower with decreasing side length. (b) An orthographic view of figure (a) in side length versus temperature change space. As the side length decreases, there is an exponential increase in cooling required to induce a bistable laminate.

Figures 3b-3c show that all three bifurcation points (B1)-(B3) and their inverted analogues (B1i)-(B3i) arise as a result of instabilities on the fundamental cool-down path. What is interesting is that bifurcation points (B2) and (B3) arise concurrently at a double bifurcation point as shown in the inset of Figure 3c. On a snap-through diagram (F vs. w) bifurcation points (B2)/(B3i) and (B3)/(B2i) first appear at the two cusp catastrophes $dT = -17.0\,\mathrm{K}$ as four unique points. With further cooling to $dT = -17.9\,\mathrm{K}$ two of these bifurcation points, (B3) and (B3i), then coincide at a single point. Note that the connection of (B2) to (B3i) and (B3) to (B2i) depicted in the loci of bifurcation points of Figure 3c mirrors their connection by the bifurcation branches on the snap-through diagram of Figure 2d. Finally, bifurcation points (B1) and (B1i) arise on the fundamental cool-down path at $dT = -19.8$ K such that beyond this temperature, the snap-through equilibrium path is governed by one pair of limit points, (L1) and (L1i), and three pairs of bifurcation points, (B1)/(B1i)-(B3)/(B3i).

On the other hand, limit points (L2)/(L2i) and (L3)/(L3i) do not arise because of an instability on the fundamental cool-down path. Figure 3d shows that limit points (L2) and (L3) are connected, and by symmetry, so must be their inverted analogues (L2i) and (L3i). As the extent of post-cure cool-down is decreased, these two pairs of limit points move closer to each other, finally colliding and vanishing at the cusp catastrophe located at $dT = -155.1\,\mathrm{K}$. This means that the multi-snap event described above does not exist for cool-down temperatures $dT > -155.1\,\mathrm{K}$ because the localised region of positive slope is eliminated. Figure 3d shows another cusp catastrophe, this time involving limit points (L4) and (L4i) which collide at the final bifurcation point on the fundamental cool-down path $dT = -167.7\,\mathrm{K}$. Consequently, the localised feature of the snap-through equilibrium path defined by limit points (L4) and (L4i) is straightened out for $dT > -167.7\,\mathrm{K}$.

Finally, we would like to investigate how the snap-through behaviour evolves with the side length of the laminate. The baseline design considered above featured a side length of $0.25\,\mathrm{m}$ and this is now systematically varied in the generalised path-following algorithm using two possible approaches. From the cool-down pitchfork diagram (Figure 2a) we know that snap-through can only occur beyond the first instability point on the fundamental cool-down path, *i.e.* when the panel transitions from the saddle-like

shape to one of two cylindrical shapes. Hence, we use the generalised path-following algorithm to trace the locus of this first pitchfork bifurcation point with decreasing side length. Figure 4a shows this locus as a three-dimensional view in side length - dT - w space, whereas Figure 4b shows the same plot as an orthographic projection in side length - dT space ($w = 0$ along the entire locus). It is clear that the shorter the side length, the greater the degree of cool-down to initiate bistability. In fact, the relationship between side length and the first critical temperature is exponential. Initially, decreasing the side length only requires a marginal increase in cooling before the saddle-like shape becomes unstable, but for side lengths smaller than $0.1\,\mathrm{m}$ the degree of cooling required increases rapidly and approaches infinity as the side length tends to $0\,\mathrm{m}$. In a similar manner, we could pose the question of how the two cylindrical shapes at room temperature ($dT = -180\,\mathrm{K}$) evolve with decreasing side length. The V-shaped response in Figure 4a shows that with decreasing side length the two cylindrical shapes become shallower until these shapes vanish completely for a side length of $0.038\,\mathrm{m}$, which incidentally, is the point where this path intersects the locus of bifurcation points. Hence, post-cure cooling of an identical panel with side length of $0.035\,\mathrm{m}$ does not lead to a bistable laminate. Finally, note that by following a single critical point with respect to another parameter this useful design information has been established without recourse to expensive nonlinear parametric studies.

5 CONCLUSIONS

Generalised path-following combines a numerical continuation algorithm with the geometrical versatility of the finite element method. The advantage of this technique over standard path-following algorithms, ubiquitous in commercial finite element codes, is that any parameter influencing the structure, be it load, geometrical dimensions or constitutive properties, *etc.* can be followed on a multi-dimensional solution manifold. Furthermore, critical instability points are readily isolated and their sensitivity with respect to other parameters established. Finally, secondary paths in the vicinity of bifurcation points are easily determined and then explored.

It has been shown that such an algorithm is perfectly suited to the analysis and design of bistable composite laminates for morphing applications. These novel structures are fundamentally driven by instabilities as they typically rely on postbuckled stress states, and the snap-through phenomenon is itself a catastrophic event. We have shown here that the full complexity of a multi-snap event is robustly captured by generalised path-following. Furthermore, the ability to follow loci of instability points with respect to additional parameters can yield invaluable insight into the underlying physics of the multistable phenomena, establish the sensitivity of snap-through points with respect to initial imperfections, and be used for rapid design studies.

ACKNOWLEDGEMENTS

This work was funded by the Engineering and Physical Sciences Research Council under the grant number EP/MO13170/1 at the University of Bristol.

REFERENCES

[1] E. Lamacchia, P. M. Weaver, E. Eckstein, and A. Pirrera. Morphing structures: non-linear composite shells with irregular planforms. In *Proceedings of the 56th AIAA/ASCE/AHS/ASC Structures, Structural Dynamics, and Materials Conference*, 2015.

[2] S. Vidoli and C. Maurini. Tristability of thin orthotropic shells with uniform initial curvature. *Proceedings of the Royal Society A: Mathematical, Physical and Engineering Science*, 464:2949–2966, 2008.

[3] S. D. Guest and S. Pellegrino. Analytical models for bistable cylindrical shells. *Proceedings of the Royal Society A: Mathematical, Physical and Engineering Science*, 462:839–854, 2006.

[4] K. A. Seffen. Morphing bistable orthotropic elliptical shallow shells. *Proceedings of the Royal Society A: Mathematical, Physical and Engineering Science*, 463:67–83, 2007.

[5] S. Vidoli. Discrete approximation of the F oppl-von Kármán shell model: from coarse to more refined models. *International Journal of Solids and Structures*, 50:1241–1252, 2013.

[6] A. Pirrera, D. Avitabile, and P. M. Weaver. Bistable plates for morphing structures: a refined analytical approach with high-order polynomials. *International Journal of Solids and Structures*, 47:3412–3425, 2010.

[7] E. Eckstein, A. Pirrera, and P. M. Weaver. Multi-mode morphing using initially curved composite plates. *Composite Structures*, 109:240–245, 2014.

[8] M. J. Sewell. On the connection between stability and the shape of the equilibrium surface. *Journal of the Mechanics and Physics of Solids*, 14:203–230, 1966.

[9] J. M. T. Thompson and G. W. Hunt. *A General Theory of Elastic Stability*. John Wiley & Sons, 1973.

[10] J. M. T. Thompson and G. W. Hunt. A bifurcation theory for the instabilities of optimization and design. *Synthese*, 36(3):315–351, 1977.

[11] J. M. T. Thompson. Catastrophe theory in mechanics: progress or digression. *Journal of Structural Mechanics*, 10(2):167–175, 1982.

[12] W. C. Rheinboldt. Numerical analysis of continuation methods for nonlinear structural problems. *Computers and Structures*, 13:103–113, 1981.

[13] W. C. Rheinboldt. On the computation of multi-dimensional solution manifolds of parametrized equations. *Numerische Mathematik*, 53:165–181, 1988.

[14] A. Eriksson. Equilibrium subsets for multi-parametric structural analysis. *Computer Methods in Applied Mechanics and Engineering*, 140:305–327, 1997.

[15] A. Eriksson. Structural instability analyses based on generalised path-following. *Computer Methods in Applied Mechanics and Engineering*, 156:45–74, 1998.

[16] M. W. Hyer. Some observations on the cured shape of thin unsymmetric laminates. *Journal of Composite Materials*, 15:175–194, 1981.

[17] E. Ramm. A plate/shell element for large deflections and rotations. In *Formulations and Computational Algorithms in Finite Element Analysis*, Cambridge, MA, USA, 1977. MIT Press.

[18] K. D. Potter, P. M. Weaver, A. Abu Seman, and S. Shah. Phenomena in the bifurcation of unsymmetric composite plates. *Composites Part A: Applied Science and Manufacturing*, 38(1):100–106, 2007.

[19] G. W. Hunt, G. J. Lord, and A. R. Champneys. Homoclinic and heteroclinic orbits underlying the post-buckling of axially-compressed cylindrical shells. *Computer Methods in Applied Mechanics and Engineering*, 170(3-4):239–251, 1999.